

# CMP Lab Report

## Zeeman Effect

Group B9\*

February 25, 2019

### Abstract

This experiment examined the normal and anomalous Zeeman effect with the aim of calculating the Bohr magneton by fitting the energy gap between spectral lines of a cadmium lamp immersed in a magnetic field, as a function of its magnitude. The first section concerns the magnet calibration and the procedure we adopted to test the magnetic field homogeneity. As far as the former is concerned, we expected the magnetic field to vary almost linearly with the current since we worked with soft ferromagnets. Regarding the latter, we measured how the magnitude of the magnetic field varied for small displacements in the region occupied by the cadmium lamp. Lastly, after the global experimental apparatus has been endowed with polarizing filters, a CCD camera and a retarding lamina, several images of the splitted spectral lines have been taken in various states depending from the chosen orientation (longitudinal or traversal) of the magnets with respect to the optical axis and the configuration of the polarizing filters placed along the light path. The results consist of four estimates of the Bohr magneton and the relevant compatibility tests.

---

\*Pietro Monticone , Claudio Moroni , Alberto Mosso , Riccardo Valperga.

# Contents

<b>1 Theoretical Introduction</b>	<b>4</b>
1.1 Normal Zeeman effect . . . . .	4
1.2 Anomalous Zeeman Effect . . . . .	4
<b>2 Experimental Introduction</b>	<b>5</b>
2.1 Apparatus . . . . .	5
2.2 Procedure . . . . .	6
2.3 Uncertainty Assignment & Approximation Method . . . . .	6
<b>3 Calibration</b>	<b>8</b>
3.1 Data Collection . . . . .	8
3.2 Data Analysis & Visualization . . . . .	9
<b>4 Magnetic Field Homogeneity Test</b>	<b>11</b>
<b>5 Normal Zeeman Effect</b>	<b>13</b>
5.1 Data Collection . . . . .	13
5.2 Data Analysis & Visualization . . . . .	13
5.3 Bohr Magneton . . . . .	15
<b>6 Anomalous Zeeman Effect</b>	<b>16</b>
6.1 Data Collection . . . . .	16
6.2 Data Analysis & Visualization . . . . .	16
6.3 Bohr Magneton . . . . .	18
<b>7 Conclusions</b>	<b>19</b>
<b>8 Appendix</b>	<b>20</b>

# Nomenclature

The following list explains the symbols used within the body of the report.

## Experimental Equipment

CCD Charge-Coupled Device

## Physical Constants

$\mu_B$  Bohr Magneton

$c$  Speed of Light in the Vacuum

$e$  Electronic Charge

$h$  Plack Constant

$m_e$  Electronic Mass

## Theoretical Concepts

$\mu_{X \in \{N,A\}}^{Y \in \{T,L\}}$  Magnetic Moment in  $(X, Y)$

$\vec{B}$  Magnetic Induction

$g$  Gyromagnetic Factor

$g_{q \in \{n,a\}}$  “Normal”/“Anomalous” Gyromagnetic Factor

$I$  Electric Current

$w$  Fabry-Perot Interferometer Thickness

# 1 Theoretical Introduction

The Zeeman effect is a phenomenon where the immersion of a spectroscopic light source in a magnetic field causes the splitting of the observed spectral lines. Since a spectral line is associated to an atomic energy level, the splitting is always related to a degeneracy breaking mechanism. In an atom, degeneracy is due to the orbital angular momentum quantum number  $\ell$ , its third component  $m_\ell$  and the spin  $m_s$  ( $s = 1/2$  is fixed because electrons are fermions).

- The normal Zeeman effect is observed when the total spins of the base and target level of the transition are zero.
- The anomalous Zeeman effect is instead detected when the spins of the base and target level of the transition are not zero.

## 1.1 Normal Zeeman effect

An external magnetic field  $\vec{B}$  gives an energy contribution to each level

$$\Delta E = -\vec{\mu} \cdot \vec{B} \quad (1)$$

Where  $\vec{\mu}$  is the magnetic moment. We consider  $\vec{B}$  parallel to the z-axis, so we are only interested in  $\mu_z$ . One finds:

$$\mu_z \equiv -\frac{e}{2m} L_z = -\frac{e}{2m} \hbar m_\ell g_\ell \quad (2)$$

Where  $g_\ell$  (orbital gyromagnetic factor) is a constant equal to 1. Thus:

$$\Delta E = -\mu_z B = \frac{e\hbar}{2m} m_\ell B = \mu_B m_\ell B \quad (3)$$

Where  $\mu_B$  is the Bohr magneton, whose theoretical value is  $\mu_B = 9.27 \times 10^{-24} \text{ JT}^{-1}$ . Since  $\Delta E$  depends on  $m_\ell$ , degeneracy in  $m_\ell$  is broken and thus spectral lines split.

## 1.2 Anomalous Zeeman Effect

When spin is involved, the expression for  $\vec{\mu}$  to use is

$$\vec{\mu} = -\frac{eg_\ell}{2m} \vec{L}_J - \frac{eg_s}{2m} \vec{S}_J \quad (4)$$

Where  $\vec{L}_J$  and  $\vec{S}_J$  are the projections of  $\vec{L}$  and  $\vec{S}$  along the total angular momentum  $\vec{J} := \vec{L} + \vec{S}$ , and  $g_s$  is about 2. One finds:

$$\vec{\mu} = -\frac{e}{2m} g_{jls} \vec{J} \quad (5)$$

Where

$$g_{jls} = \frac{3j(j+1) - \ell(\ell+1) + s(s+1)}{2j(j+1)} \quad (6)$$

Pointing  $\vec{B}$  along the  $z$ -axis, we have  $\mu_z = -\frac{e\hbar}{2m}g_{j\ell s}m_j = -\mu_B g_{j\ell s}m_j$ , thus

$$\Delta E = -\vec{\mu} \cdot \vec{B} = \mu_z B = \mu_B g_{j\ell s}m_j B \quad (7)$$

When considering the anomalous Zeeman effect, both spinorial and orbital degeneracies are broken, giving rise to even more splitting.

## 2 Experimental Introduction

### 2.1 Apparatus

The apparatus consists of two electromagnetic components with ferromagnetic core connected to a current generator, an amperometer and a magnetometer as represented by the circuit in [Figure 1](#)<sup>1</sup>.

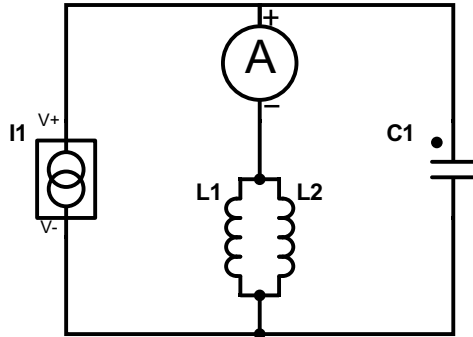


**Figure 1**

An optical bench endowed with a cadmium spectroscopic light source inserted between the electromagnets discussed above, a diaphragm, a Fabry-Perot interferometer, a wavelength filter, a polarizer, a retarding lamina and a CCD camera has been used. A particular wavelength range of the light coming from the source was selected via the filter before entering the interferometer. The Fabry-Perot interferometer enables the diffraction of an input wavelength in a series of circular spectral lines. As the filter acts on a wavelength range, we could observe the splitting of a wavelength into two or three<sup>2</sup> or six or nine<sup>3</sup>, without dealing with extra lines. The Fabry-Perot interferometer main characteristic is the following:

We have defined

$$\delta = r_{n,a}^2 - r_{n,b}^2 \text{ and } \Delta = r_{n+1,a}^2 - r_{n,a}^2,$$

where  $r_{n,a}$  is the radius of the  $n^{\text{th}}$  order spectral line corresponding to the wavelength  $a$ . We know that  $\delta$  and  $\Delta$  are approximately constant with respect to  $n$  and  $\lambda$  as far

---

<sup>1</sup>The capacity  $C$  is large and it is there for safety reasons .

<sup>2</sup>Normal longitudinal or transverse as described in [Procedure](#) .

<sup>3</sup>Anomalous longitudinal or transverse as described in [Procedure](#) .

as the same diffractogram is concerned. Moreover, by geometric means, one finds that

$$\Delta E = \frac{hc}{2\mu w} \frac{\delta}{\Delta} \quad (8)$$

where  $\mu$  is the refractive index of the interferometer and  $w$  is its thickness. So it is possible to calculate  $\Delta E$  by analyzing the images acquired from the CCD camera.

## 2.2 Procedure

The experimental procedures we have followed to observe the normal and the anomalous Zeeman effect are very similar. The magnets could be rotated, giving rise to the possibility of perpendicular and longitudinal configurations<sup>4</sup>. When considering the former, the output radiation was linearly polarized<sup>5</sup>; the latter returned circularly polarized light: the lamina was used in combinations with the polarizer. It should be said that in longitudinal configuration the  $\pi$  light component disappeared.

The wavelength  $\sim 643$  nm corresponding to  $3^1D_2 \rightarrow 2^1P_1$  transition was selected to observe the normal Zeeman effect, while the wavelength  $\sim 508$  nm corresponding to  $3^3S_1 \rightarrow 2^3P_2$  was chosen to observe the anomalous one.

At each value of the current flowing through the electromagnets three snapshots (diffractograms) of the CCD were taken: the first depicting all lines, the second and the third were retrieved after inserting the polarizer and selecting one polarization and the other. This was executed for both the normal and anomalous settings, in transverse and longitudinal configurations.

Thus for each value of current (i.e. for each value of magnetic field extrapolated from the  $B - I$  curve one got before) we had many values of  $\delta$  and  $\Delta$  (all we could get from the three CCD snapshots), whose averages were to be used to get  $\Delta E$  from [Equation 8](#). Measures of  $\delta$  and  $\Delta$  were taken on diffractograms using Motic Images Plus 3.0 software. Thus one ends up with four linear fits of  $\Delta E$  vs  $B$ , from which we could get four estimates of  $\mu_B$ , that were then compared, averaged and compared with the theoretical value. According to  $g_{jls}$ ,  $m_l$  and  $m_j$  values, we used  $\Delta E = \mu_B B$  to fit normal zeemann effect data, and  $\Delta E = \frac{1}{2}\mu_B B$  for the anomalous one.

## 2.3 Uncertainty Assignment & Approximation Method

The errors on  $\langle \delta \rangle$  and  $\langle \Delta \rangle$  have been calculated as the standard deviation which have been propagated to get the error on  $\langle \delta \rangle / \langle \Delta \rangle$ . As far as the anomalous setting is concerned, it has not been possible to distinguish the spectral lines within the same order so to directly measure the values of  $\delta$  and  $\Delta$  we decided to adopt the following method: from the  $I = 0$  diffractogram we have measured each spectral lines' thickness  $\Delta r$ . Given the hypothesis that the lines's thickness would have been conserved See [Figure 15](#) in the [Appendix](#)., we added  $\Delta r/2$  to the most internal one

---

<sup>4</sup>The orientations are referred to the optical axis .

<sup>5</sup>It's possible to choose to observe the 2 linear polarizations ( $\pi$  and  $\sigma$ ) by rotating the axis of the polarizer, no retarding lamina is needed .

and subtracted  $\Delta r/2$  to the most external one. The difference between these two values have been divided by the number of expected lines minus one.

### 3 Calibration

#### 3.1 Data Collection

In order to calibrate the magnet it is necessary to establish the dependence of the magnetic field  $B$  from the current  $I$  injected in the coils. Therefore we gradually increased and then decreased  $I$  as shown in [Table 1](#) and [Table 2](#) respectively <sup>6</sup>.

**Table 1**

$I$ [A]	$B$ [T]
$0.00 \pm 0.02$	$0.000 \pm 0.001$
$1.02 \pm 0.02$	$0.071 \pm 0.001$
$2.03 \pm 0.02$	$0.140 \pm 0.001$
$3.00 \pm 0.02$	$0.205 \pm 0.001$
$4.04 \pm 0.02$	$0.277 \pm 0.001$
$4.99 \pm 0.02$	$0.342 \pm 0.001$
$6.02 \pm 0.02$	$0.408 \pm 0.001$
$7.00 \pm 0.02$	$0.471 \pm 0.001$
$8.02 \pm 0.02$	$0.535 \pm 0.001$
$8.48 \pm 0.02$	$0.563 \pm 0.001$
$9.01 \pm 0.02$	$0.588 \pm 0.001$
$9.51 \pm 0.02$	$0.612 \pm 0.001$
$10.04 \pm 0.02$	$0.636 \pm 0.001$

$I$ [A]	$B$ [T]
$10.04 \pm 0.02$	$0.636 \pm 0.001$
$9.50 \pm 0.02$	$0.613 \pm 0.001$
$8.97 \pm 0.02$	$0.590 \pm 0.001$
$8.49 \pm 0.02$	$0.566 \pm 0.001$
$7.00 \pm 0.02$	$0.478 \pm 0.001$
$6.05 \pm 0.02$	$0.416 \pm 0.001$
$4.98 \pm 0.02$	$0.348 \pm 0.001$
$4.02 \pm 0.02$	$0.282 \pm 0.001$
$3.00 \pm 0.02$	$0.215 \pm 0.001$
$2.00 \pm 0.02$	$0.145 \pm 0.001$
$1.00 \pm 0.02$	$0.078 \pm 0.001$
$0.00 \pm 0.02$	$0.009 \pm 0.001$

**Table 2**

$I$ [A]	$B$ [T]
$0.00 \pm 0.02$	$0.009 \pm 0.001$
$0.99 \pm 0.02$	$0.072 \pm 0.001$
$1.97 \pm 0.02$	$0.138 \pm 0.001$
$3.03 \pm 0.02$	$0.208 \pm 0.001$
$4.02 \pm 0.02$	$0.276 \pm 0.001$
$5.04 \pm 0.02$	$0.345 \pm 0.001$
$6.00 \pm 0.02$	$0.409 \pm 0.001$
$7.02 \pm 0.02$	$0.475 \pm 0.001$
$8.06 \pm 0.02$	$0.540 \pm 0.001$
$8.46 \pm 0.02$	$0.561 \pm 0.001$
$9.02 \pm 0.02$	$0.590 \pm 0.001$
$9.57 \pm 0.02$	$0.616 \pm 0.001$
$10.06 \pm 0.02$	$0.637 \pm 0.001$

$I$ [A]	$B$ [T]
$10.06 \pm 0.02$	$0.637 \pm 0.001$
$9.50 \pm 0.02$	$0.613 \pm 0.001$
$8.97 \pm 0.02$	$0.590 \pm 0.001$
$8.49 \pm 0.02$	$0.566 \pm 0.001$
$7.00 \pm 0.02$	$0.478 \pm 0.001$
$6.05 \pm 0.02$	$0.416 \pm 0.001$
$4.98 \pm 0.02$	$0.348 \pm 0.001$
$4.02 \pm 0.02$	$0.282 \pm 0.001$
$3.00 \pm 0.02$	$0.215 \pm 0.001$
$2.00 \pm 0.02$	$0.145 \pm 0.001$
$1.00 \pm 0.02$	$0.078 \pm 0.001$
$0.00 \pm 0.02$	$0.009 \pm 0.001$

<sup>6</sup>Instrumental sensitivities:  $\Delta I = \pm 0.02$  A ;  $\Delta B = \pm 0.001$  T .

### 3.2 Data Analysis & Visualization

For sufficiently high values of  $I$  the magnet exhibits a non-linear response which constrains us to fit the datasets with both linear and parabolic models in different domains as shown in Figure 2 and 3.

$$\begin{cases} f(I) = \mathbf{a}I + \mathbf{b} & \forall I \leq 7.00 \text{ A} \\ g(I) = \mathbf{a}_p I^2 + \mathbf{b}_p I + \mathbf{c}_p & \forall I > 7.00 \text{ A} \end{cases}$$

$$\begin{cases} f(I) = \mathbf{p}_0 I + \mathbf{p}_1 & \forall I \leq 7.00 \text{ A} \\ g(I) = \mathbf{a}_p I^2 + \mathbf{b}_p I + \mathbf{c}_p & \forall I > 7.00 \text{ A} \end{cases}$$

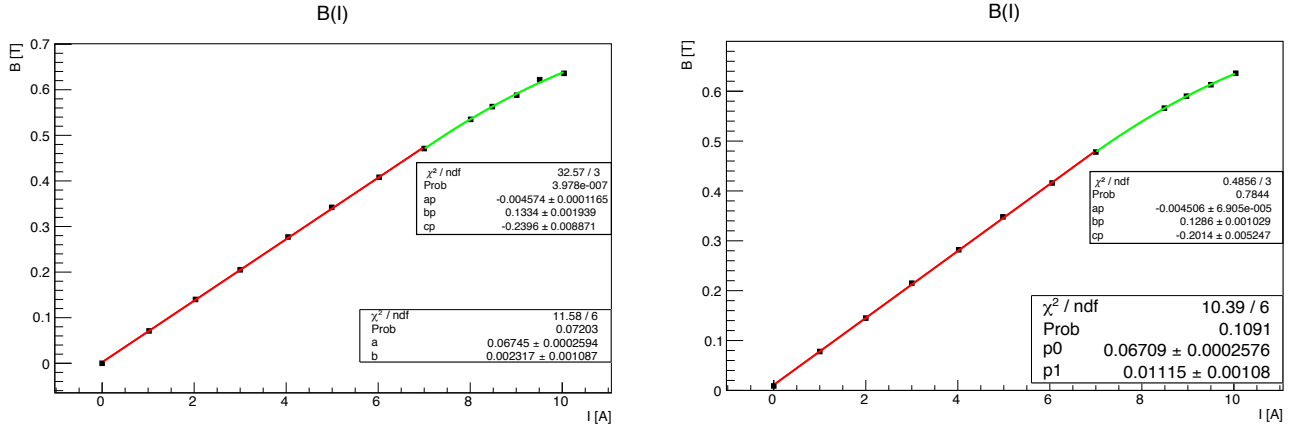


Figure 2

$$\begin{cases} f(I) = \mathbf{a}I + \mathbf{b} & \forall I \leq 7.02 \text{ A} \\ g(I) = \mathbf{a}_p I^2 + \mathbf{b}_p I + \mathbf{c}_p & \forall I > 7.02 \text{ A} \end{cases}$$

$$\begin{cases} f(I) = \mathbf{p}_0 I + \mathbf{p}_1 & \forall I \leq 7.00 \text{ A} \\ g(I) = \mathbf{a}_p I^2 + \mathbf{b}_p I + \mathbf{c}_p & \forall I > 7.00 \text{ A} \end{cases}$$

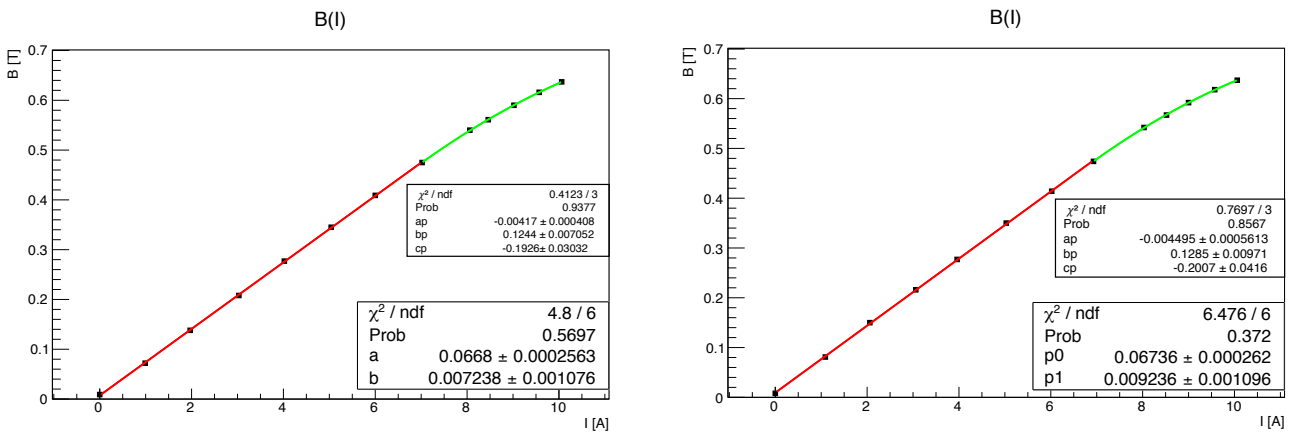
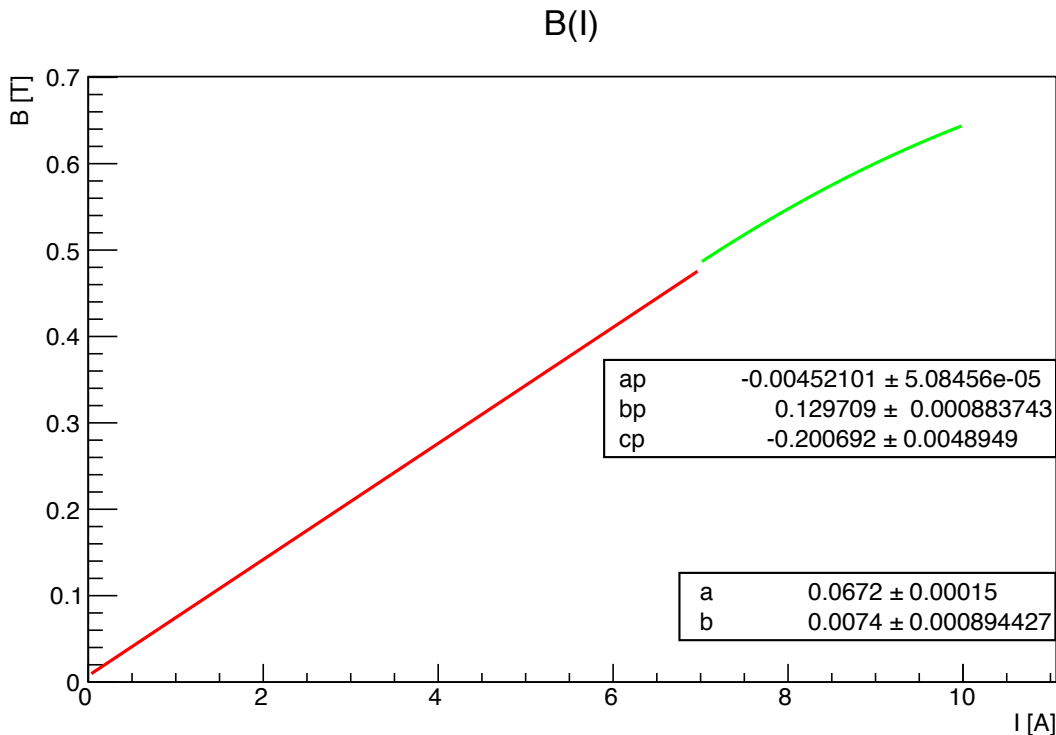


Figure 3

The final calibration curve reported in [Figure 4](#) has been calculated as follows:

1. the four values of each parameter have been averaged ;
2. the compatibility test between every single one with the global average has been computed ;
3. the compatible ones has been used to get the final curve and their average has been shown to be compatible with the global one.

It might be interesting to observe that, although the magnet we have worked with was a soft ferromagnet, the final calibration curve exhibits a residual magnetization measuring approximately 7 mT .



**Figure 4**

From now on the compatibility tests will be evaluated according to the following rules:

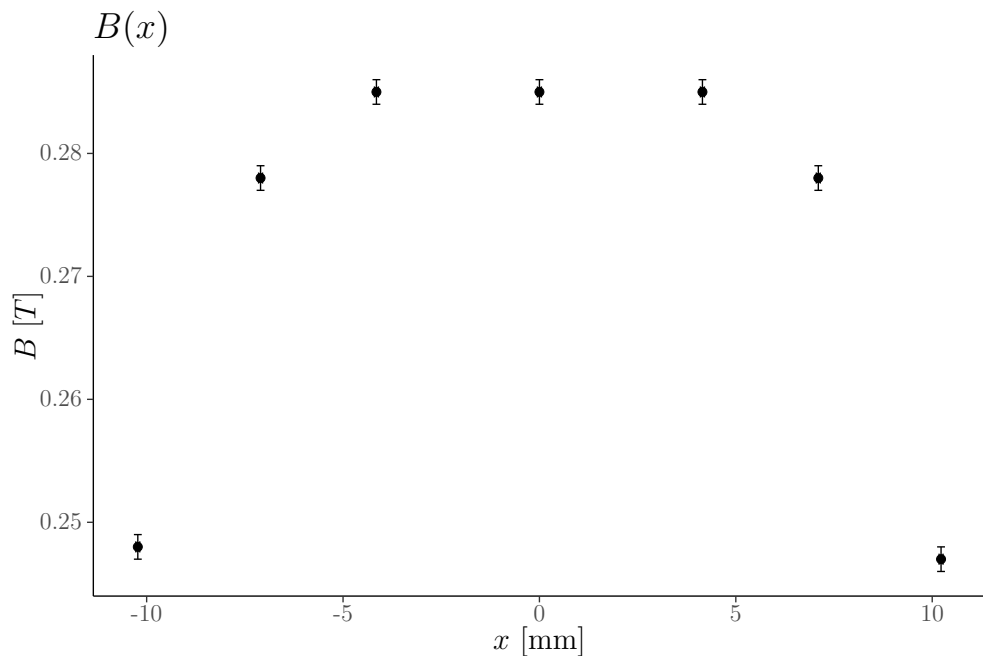
$$\begin{cases} Z = \frac{|y-x|}{\sqrt{\delta y^2 + \delta x^2}} \\ Z_c = 1.96 \quad (\alpha = 0.05) \\ \text{Compatibility condition: } Z < Z_c . \end{cases}$$

## 4 Magnetic Field Homogeneity Test

As anticipated in the [Experimental Introduction](#), in order to assign a proper uncertainty to the magnitude of the magnetic field  $B$ , it is necessary to evaluate its uniformity between the expansions. Therefore we took five measures of  $B$  along a chosen horizontal diameter  $x$ , which have been reported in [Table 3](#) and other five along the vertical  $y$  reported in [Table 4](#). The relevant scatterplots have been displayed in [Figure 5](#) and [6](#) respectively<sup>7</sup>.

**Table 3**

$I [A]$	$x [\text{mm}]$	$B [T]$
$4.20 \pm 0.02$	$-10.23 \pm 0.05$	$0.248 \pm 0.001$
	$-7.10 \pm 0.05$	$0.278 \pm 0.001$
	$-4.15 \pm 0.05$	$0.285 \pm 0.001$
	$0.00 \pm 0.05$	$0.285 \pm 0.001$
	$4.15 \pm 0.05$	$0.285 \pm 0.001$
	$7.10 \pm 0.05$	$0.278 \pm 0.001$
	$10.23 \pm 0.05$	$0.247 \pm 0.001$

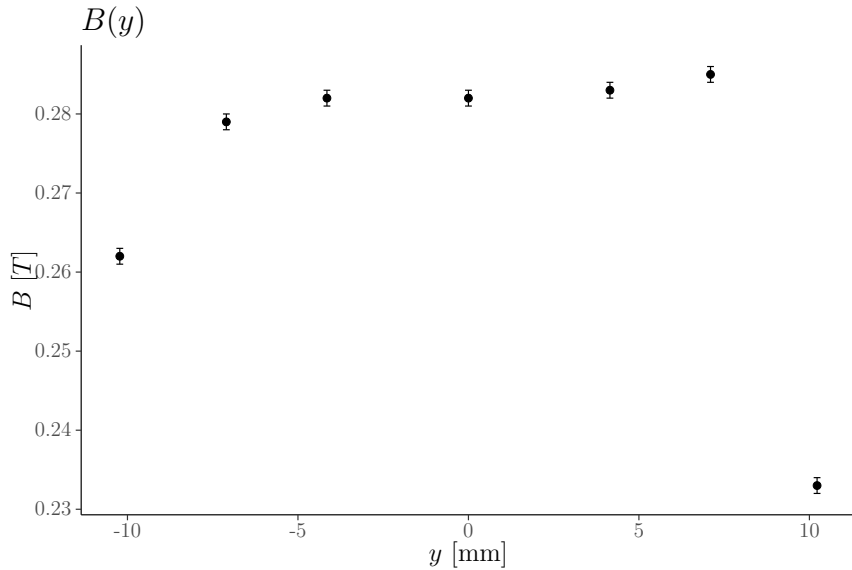


**Figure 5**

<sup>7</sup>Instrumental sensitivities:  $\Delta x = \Delta y = 0.05 \text{ mm}$ .

**Table 4**

$I [A]$	$y [\text{mm}]$	$B [T]$
$4.13 \pm 0.02$	$-10.23 \pm 0.05$	$0.262 \pm 0.001$
	$-7.10 \pm 0.05$	$0.279 \pm 0.001$
	$-4.15 \pm 0.05$	$0.282 \pm 0.001$
	$0.00 \pm 0.05$	$0.282 \pm 0.001$
	$4.15 \pm 0.05$	$0.283 \pm 0.001$
	$7.10 \pm 0.05$	$0.285 \pm 0.001$
	$10.23 \pm 0.05$	$0.233 \pm 0.001$

**Figure 6**

Since the spectroscopic lamp was taller than larger, in order to evaluate the uncertainty of the magnetic field along the  $x$  coordinate we have considered only the first four measures around the central position, while to evaluate it along the  $y$  coordinate we have considered all the measurements and calculated the maximum semi-dispersions  $\Delta_B^x = 0.007 T$  and  $\Delta_B^y = 0.052 T$ .

Then we have computed the average of the semi-dispersions and the relative error with respect to the maximum value of  $B = 0.285 T$ , whose results have been reported in [Table 5](#).

**Table 5**

$\Delta_B^x [T]$	$\Delta_B^y [T]$	$\langle \Delta_B \rangle [T]$	$\Delta_{\text{rel}}$
0.007	0.052	0.0295	0.1035087719

From now on the error assigned to the magnetic field will be  $\Delta_B = B\Delta_{\text{rel}}$ , unless the error propagation derived from the calibration curve yields a larger value.

## 5 Normal Zeeman Effect

### 5.1 Data Collection

The data regarding the transverse and longitudinal configurations have been collected and reported in [Table 6](#) and [7](#) respectively. The values of  $B$  have been derived from those of  $I$  in [Calibration Curve](#), while  $\frac{\langle \delta \rangle}{\langle \Delta \rangle}$  has been calculated as described in the [Experimental Introduction](#). Since  $I$  wasn't constant during the data collection procedure,  $\Delta I = I\Delta_I^{\text{semi}}$ , unless the instrumental sensitivity was larger .

### 5.2 Data Analysis & Visualization

The datasets concerning the transverse and longitudinal configurations have been fit with the linear model  $f(B) = p_0B + p_1$  and plotted in [Figure 7](#) and [8](#), together with the respective fit parameters  $p_0$  and  $p_1$  .

**Table 6**

$I$ [A]	$B$ [T]	$\frac{\langle \delta \rangle}{\langle \Delta \rangle}$
$2.61 \pm 0.02$	$0.183 \pm 0.019$	$0.061 \pm 0.004$
$4.92 \pm 0.02$	$0.338 \pm 0.035$	$0.125 \pm 0.007$
$5.84 \pm 0.02$	$0.400 \pm 0.041$	$0.158 \pm 0.003$
$6.83 \pm 0.02$	$0.466 \pm 0.048$	$0.188 \pm 0.006$
$7.225 \pm 0.025$	$0.500 \pm 0.052$	$0.198 \pm 0.006$
$7.92 \pm 0.02$	$0.543 \pm 0.056$	$0.221 \pm 0.004$
$8.91 \pm 0.02$	$0.596 \pm 0.062$	$0.233 \pm 0.006$
$9.92 \pm 0.02$	$0.641 \pm 0.066$	$0.263 \pm 0.009$

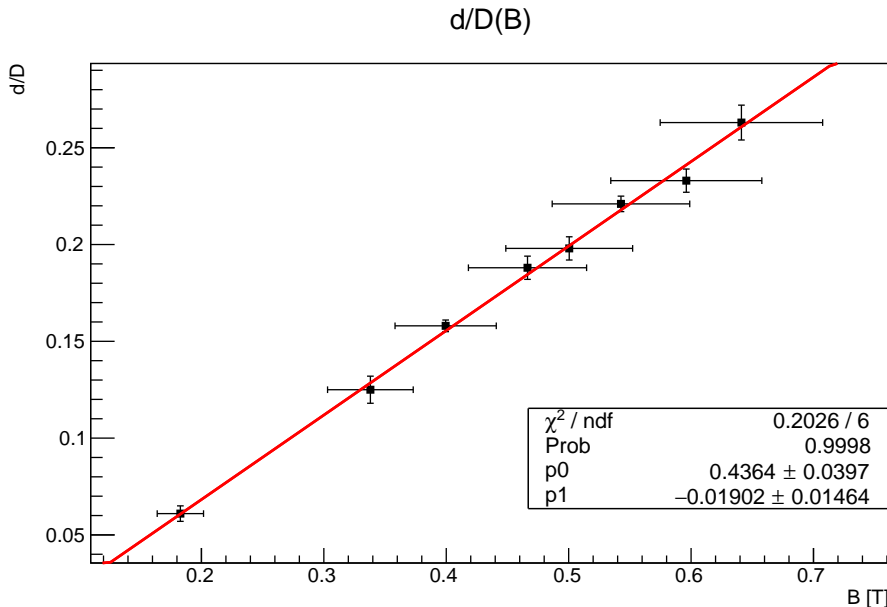


**Figure 7:** Transverse

**Table 7**

$I$ [A]	$B$ [T]	$\frac{\langle \delta \rangle}{\langle \Delta \rangle}$
$2.69 \pm 0.02$	$0.188 \pm 0.019$	$0.070 \pm 0.002$
$4.84 \pm 0.02$	$0.333 \pm 0.034$	$0.140 \pm 0.003$
$5.91 \pm 0.02$	$0.404 \pm 0.082$	$0.165 \pm 0.002$
$6.93 \pm 0.03$	$0.473 \pm 0.049$	$0.192 \pm 0.002$
$7.23 \pm 0.02$	$0.500 \pm 0.052$	$0.202 \pm 0.010$
$7.86 \pm 0.02$	$0.539 \pm 0.056$	$0.218 \pm 0.002$
$8.83 \pm 0.02$	$0.592 \pm 0.061$	$0.237 \pm 0.006$
$9.80 \pm 0.02$	$0.636 \pm 0.066$	$0.263 \pm 0.009$

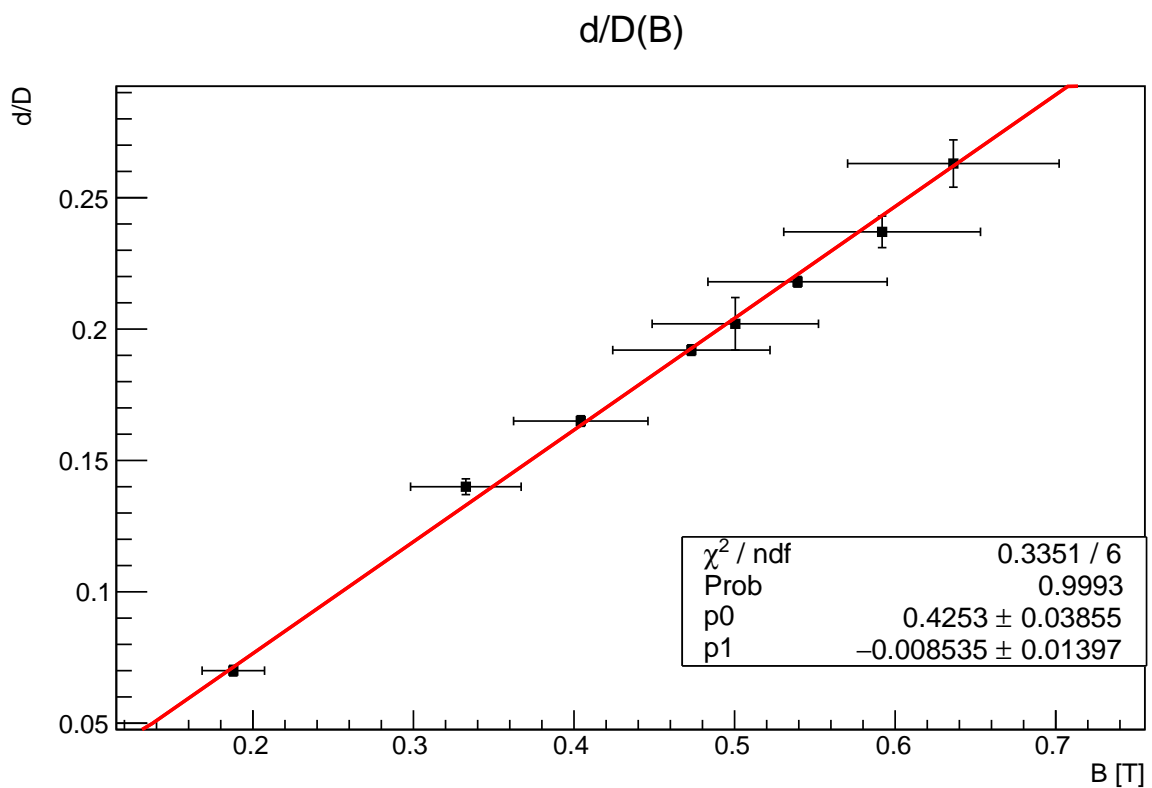


**Figure 8:** Longitudinal

### 5.3 Bohr Magnetons

Now it is possible to calculate the Bohr magneton for both configurations

$$\mu_N^T = (\mathbf{p}_0^T \pm \delta \mathbf{p}_0^T) \frac{hc}{2g_n\mu_n w} \quad \text{and} \quad \mu_N^L = (\mathbf{p}_0^L \pm \delta \mathbf{p}_0^L) \frac{hc}{2g_n\mu_n w}$$

since we know

- $h = 6.626070040 \times 10^{-34}$  Js Planck constant
- $c = 299792458$  ms $^{-1}$  speed of light in the vacuum
- $g_n = 1$  gyromagnetic factor
- $\mu_n = 1.4560$  refractive index
- $w = 0.003$  m thickness
- $\mathbf{p}_0^T = 0.436 \pm 0.040$  T $^{-1}$  transverse slope
- $\mathbf{p}_0^L = 0.425 \pm 0.039$  T $^{-1}$  longitudinal slope .

The compatibility between  $\mu_N^T$  and  $\mu_N^L$  has been tested as displayed in [Table 8](#).

**Table 8**

$\mu_N^T$ [JT $^{-1}$ ]	$\mu_N^L$ [JT $^{-1}$ ]	$Z$	Compatibility
$(9.91 \pm 0.91) \times 10^{-24}$	$(9.66 \pm 0.89) \times 10^{-24}$	0.20	✓

Since the result has been positive, we have calculated the weighted average  $\langle \mu_N \rangle$  and tested against the theoretical value  $\mu_B$  as shown in [Table 9](#).

**Table 9**

$\langle \mu_N \rangle$ [JT $^{-1}$ ]	$\mu_B$ [JT $^{-1}$ ]	$Z$	Compatibility
$(9.79 \pm 0.63) \times 10^{-24}$	$9.27 \times 10^{-24}$	0.41	✓

## 6 Anomalous Zeeman Effect

### 6.1 Data Collection

The data regarding the transverse and longitudinal configurations have been collected and reported in [Table 10](#) and [11](#) respectively. The values of  $B$  have been derived from those of  $I$  in [Calibration Curve](#), while  $\frac{\langle \delta \rangle}{\langle \Delta \rangle}$  has been calculated as described in the [Experimental Introduction](#).

### 6.2 Data Analysis & Visualization

The datasets concerning the transverse and longitudinal configurations have been fit with the linear model  $f(B) = p_0 B + p_1$  and plotted in [Figure 9](#) and [10](#), together with the respective fit parameters  $p_0$  and  $p_1$ .

**Table 10**

$I$ [A]	$B$ [T]	$\frac{\langle \delta \rangle}{\langle \Delta \rangle}$
$5.75 \pm 0.04$	$0.394 \pm 0.041$	$0.062 \pm 0.002$
$6.74 \pm 0.02$	$0.460 \pm 0.048$	$0.081 \pm 0.021$
$7.275 \pm 0.025$	$0.504 \pm 0.052$	$0.098 \pm 0.019$
$7.82 \pm 0.02$	$0.537 \pm 0.056$	$0.086 \pm 0.034$
$8.795 \pm 0.095$	$0.590 \pm 0.061$	$0.096 \pm 0.030$
$9.95 \pm 0.04$	$0.642 \pm 0.066$	$0.082 \pm 0.032$

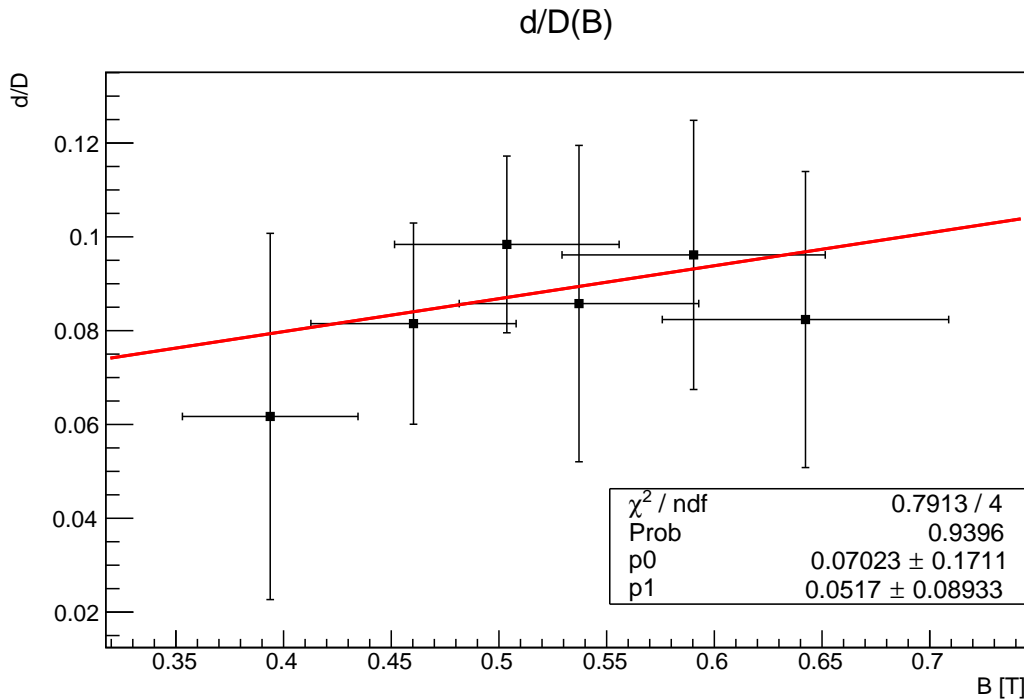


**Figure 9:** Transverse

**Table 11**

$I [A]$	$B [T]$	$\frac{\langle \delta \rangle}{\langle \Delta \rangle}$
$7.31 \pm 0.02$	$0.506 \pm 0.052$	$0.057 \pm 0.011$
$7.85 \pm 0.02$	$0.539 \pm 0.056$	$0.069 \pm 0.012$
$8.32 \pm 0.02$	$0.565 \pm 0.059$	$0.088 \pm 0.017$
$8.84 \pm 0.02$	$0.593 \pm 0.061$	$0.128 \pm 0.031$
$9.415 \pm 0.025$	$0.620 \pm 0.064$	$0.147 \pm 0.022$
$9.99 \pm 0.02$	$0.644 \pm 0.067$	$0.130 \pm 0.022$

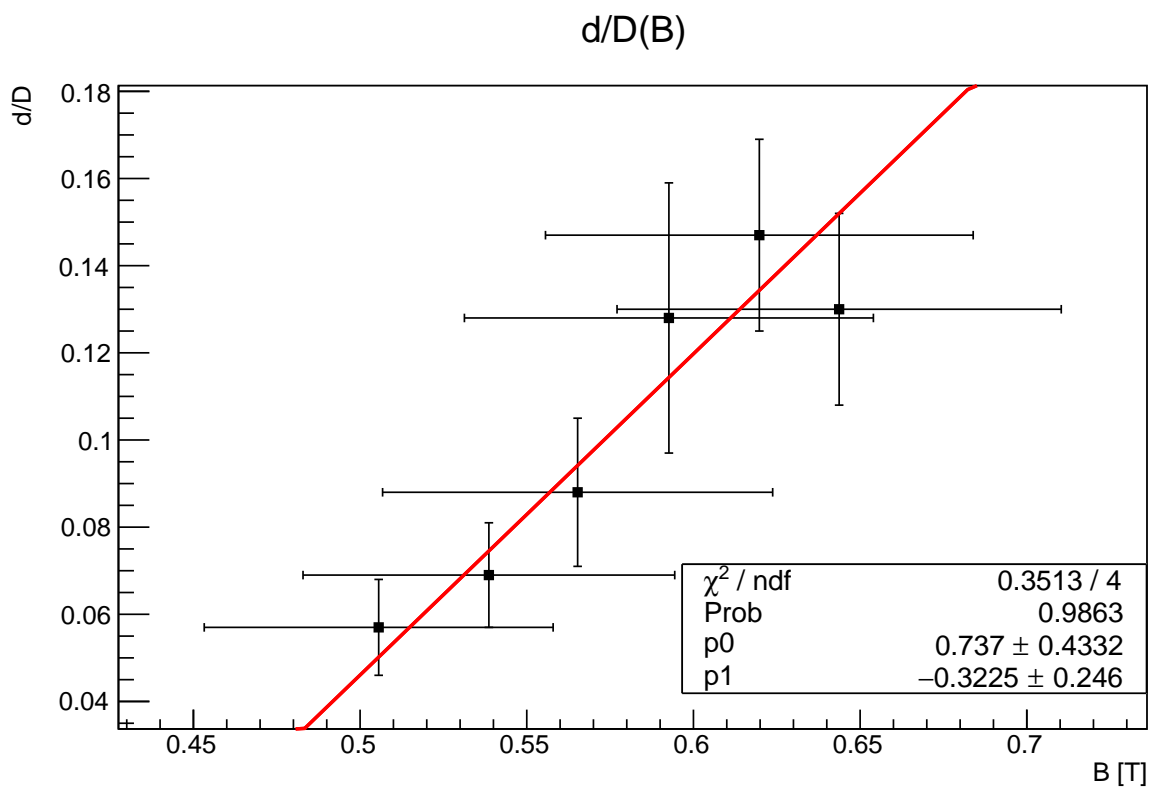


**Figure 10:** Longitudinal

### 6.3 Bohr Magnetons

Now it is possible to calculate the Bohr magneton for both configurations

$$\mu_A^T = (\mathbf{p}_0^T \pm \delta \mathbf{p}_0^T) \frac{hc}{2g_a \mu_a w} \quad \text{and} \quad \mu_A^L = (\mathbf{p}_0^L \pm \delta \mathbf{p}_0^L) \frac{hc}{2g_a \mu_a w}$$

since we know

- $h = 6.626070040 \times 10^{-34}$  Js Plack constant
- $c = 299792458$  ms $^{-1}$  speed of light in the vacuum
- $g_a = 1/2$  gyromagnetic factor
- $\mu_a = 1.4519$  refractive index
- $w = 0.003$  m thickness
- $\mathbf{p}_0^T = 0.070 \pm 0.171$  T $^{-1}$  transverse slope
- $\mathbf{p}_0^L = 0.737 \pm 0.433$  T $^{-1}$  longitudinal slope .

The compatibility between  $\mu_A^T$  and  $\mu_A^L$  has been tested as displayed in [Table 12](#).

**Table 12**

$\mu_A^T$ [JT $^{-1}$ ]	$\mu_A^L$ [JT $^{-1}$ ]	$Z$	Compatibility
$(3.20 \pm 7.80) \times 10^{-24}$	$(33.61 \pm 19.75)$	1.43	✓

Since the result has been positive, we have calculated the weighted average

$$\langle \mu_A \rangle = 7.30 \pm 7.25 \times 10^{-24} \text{ JT}^{-1}.$$

Then the compatibility test between  $\langle \mu_A \rangle$  and  $\langle \mu_N \rangle$  has been computed and displayed in [Table 13](#).

**Table 13**

$\langle \mu_A \rangle$ [JT $^{-1}$ ]	$\langle \mu_N \rangle$ [JT $^{-1}$ ]	$Z$	Compatibility
$(7.30 \pm 7.25) \times 10^{-24}$	$(9.79 \pm 6.63) \times 10^{-24}$	0.34	✓

Since the result has been positive, we have calculated the global weighted average

$$\langle \mu \rangle = 9.77 \pm 0.63 \times 10^{-24} \text{ JT}^{-1}$$

which has been tested against the theoretical value  $\mu_B$  as shown in [Table 14](#).

**Table 14**

$\langle \mu \rangle$ [JT $^{-1}$ ]	$\mu_B$ [JT $^{-1}$ ]	$Z$	Compatibility
$(9.77 \pm 0.63) \times 10^{-24}$	$9.27 \times 10^{-24}$	0.79	✓

## 7 Conclusions

We have analyzed two important phenomena concerning the cadmium energy level transitions: the normal and the anomalous Zeeman effects. Then we have calibrated the apparatus and calculated the  $(I, B)$  relation displayed in Calibration. The uncertainty  $\Delta B$  has been computed taking into account the magnetic field dishomogeneity. There were many sources of errors:

- experimental limitations mostly represented by the reduced resolutions of CCD and large errors on B and delta.
- in the anomalous setting, the data collection has been made quite problematic by the effective indistinguishability of peaks , the consequent overlap of many spectral lines and the non-negligible thickness of peaks (estimated without injected current).

For these reasons,in order to estimate the lines' position we adopted an approximation method (described in detail in the [Experimental Introduction](#)) which inevitably amplified the uncertainty on the fit parameters and therefore on the Bohr magneton. However we obtained four estimates of the magneton so that all the relevant compatibility tests (among them and with the theoretically expected value) yielded positive results. This allowed us to compute the weighted average representing our most reliable estimate.

## 8 Appendix

The diffractograms are arranged according to the following rule:

Normal Transverse

Normal Longitudinal

Anomalous Transverse

Anomalous Longitudinal

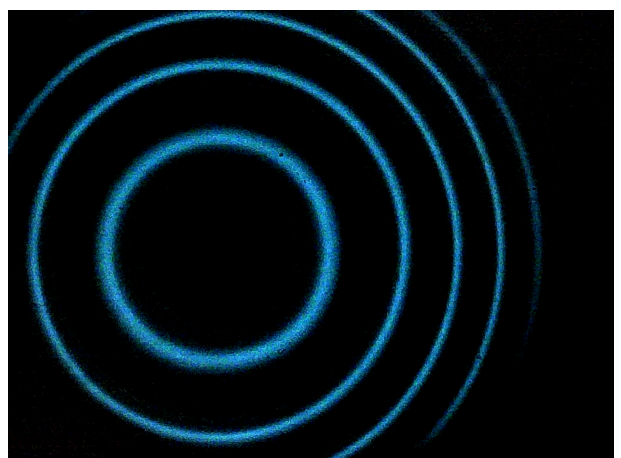
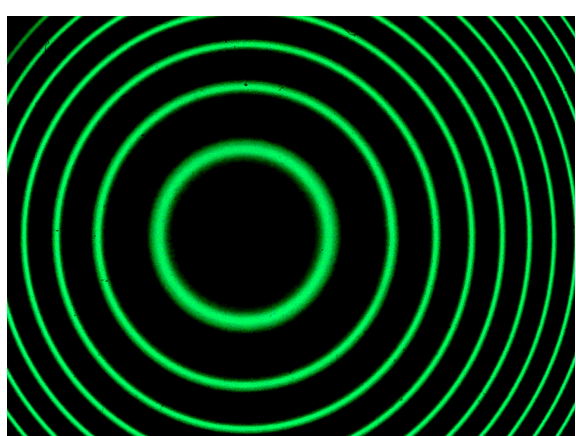
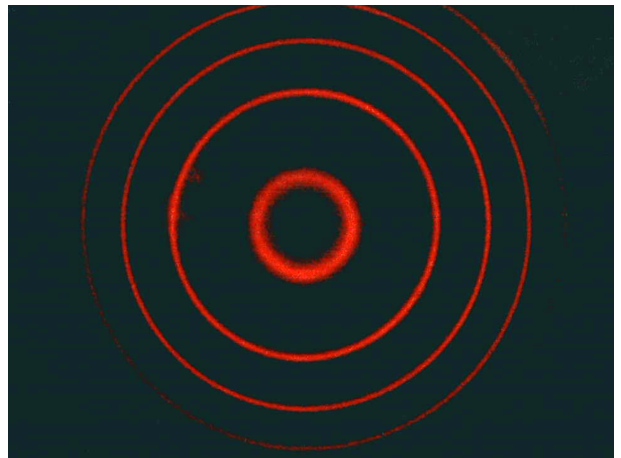


**Figure 11:**  $I = 0 \text{ A}$

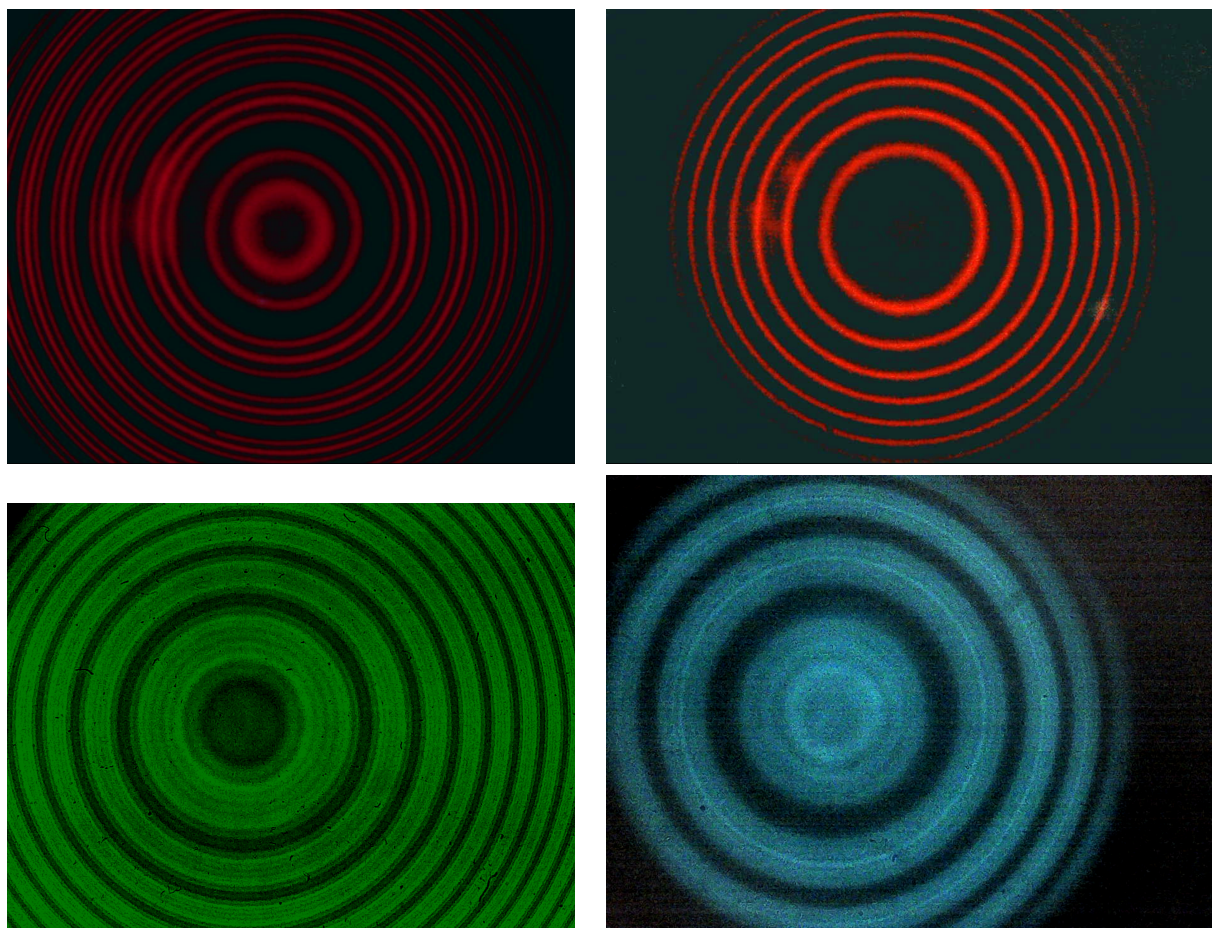


**Figure 12:** No Polarization

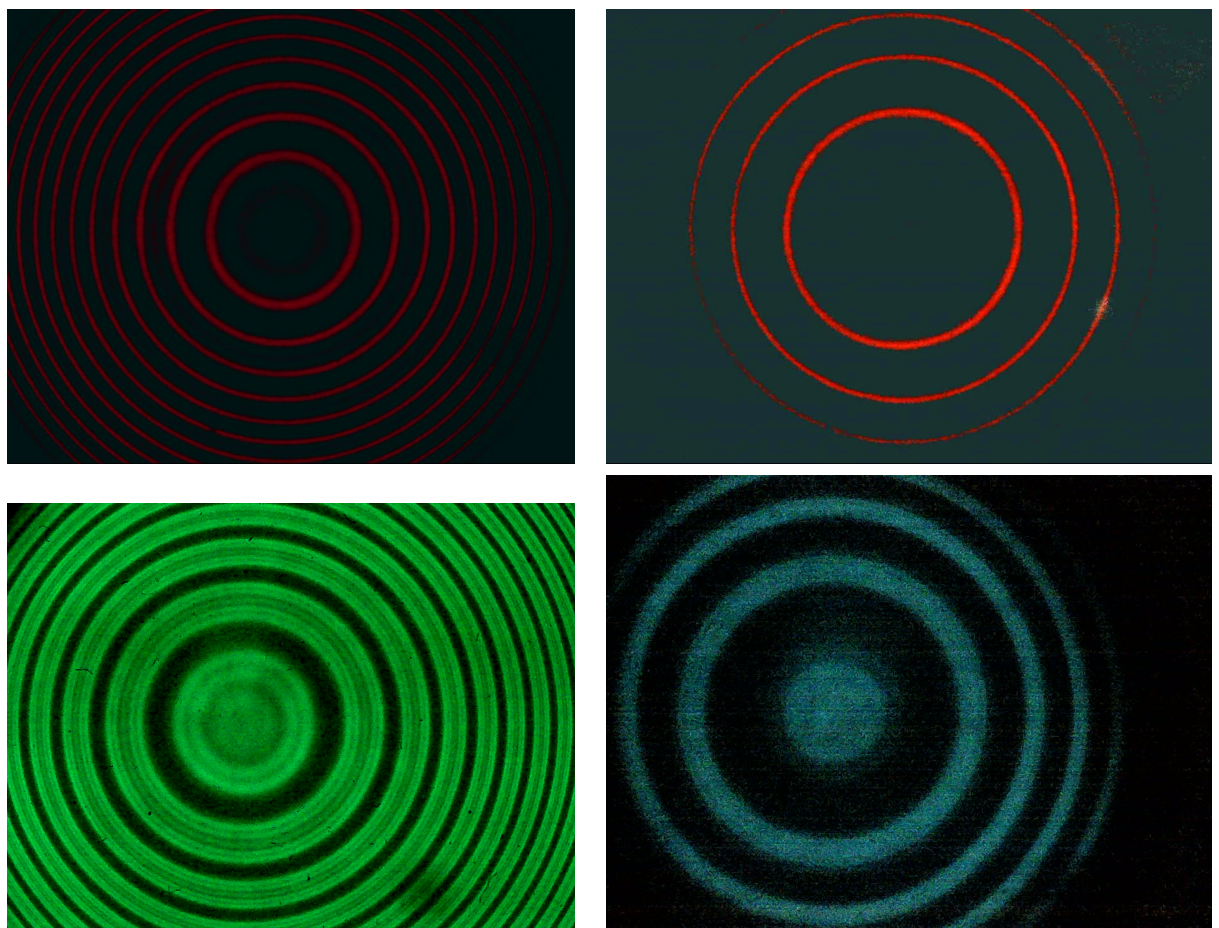


**Figure 13:** Polarization  $\sigma$  in Transverse and  $\sigma^-$  in Longitudinal

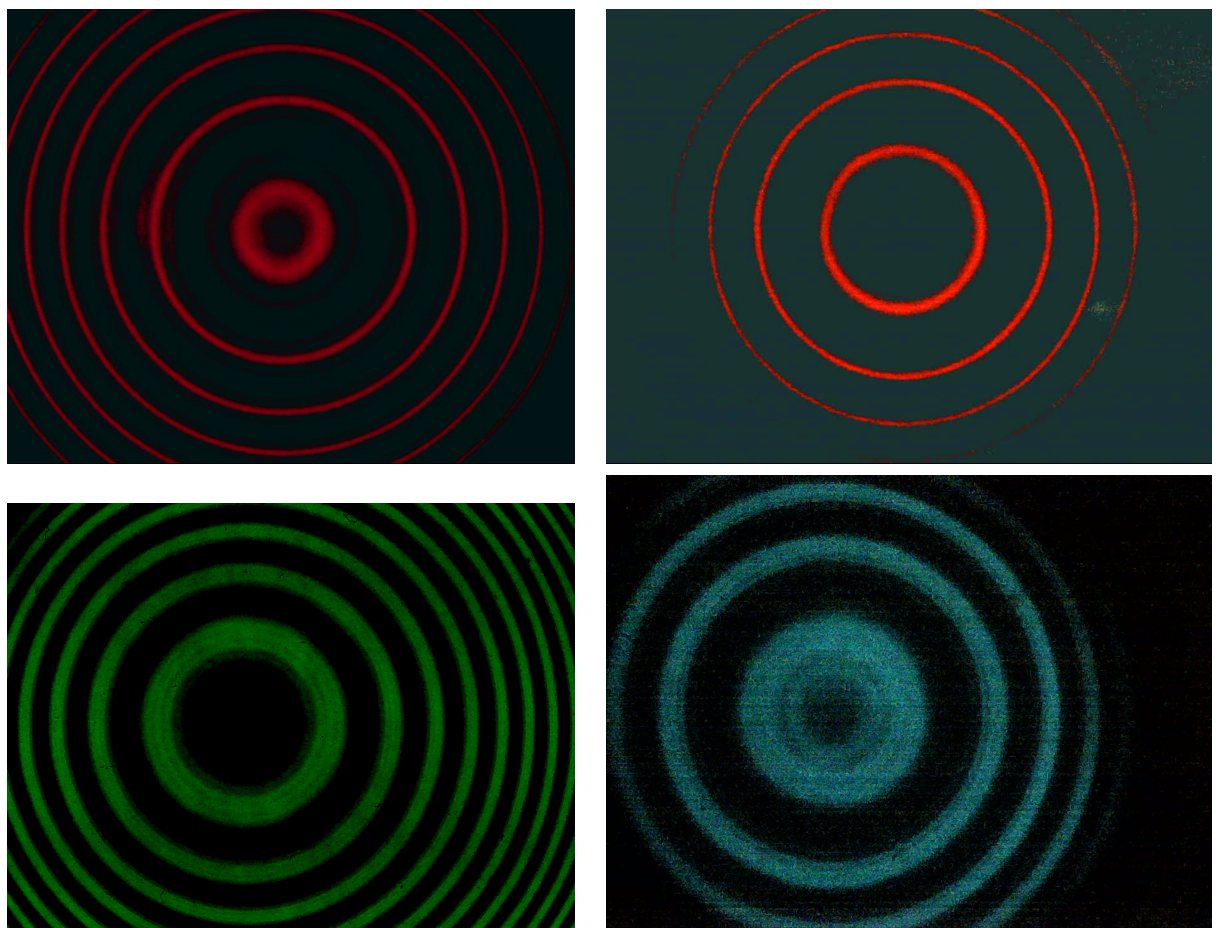


**Figure 14:** Polarization  $\pi$  in Transverse and  $\sigma^+$  in Longitudinal

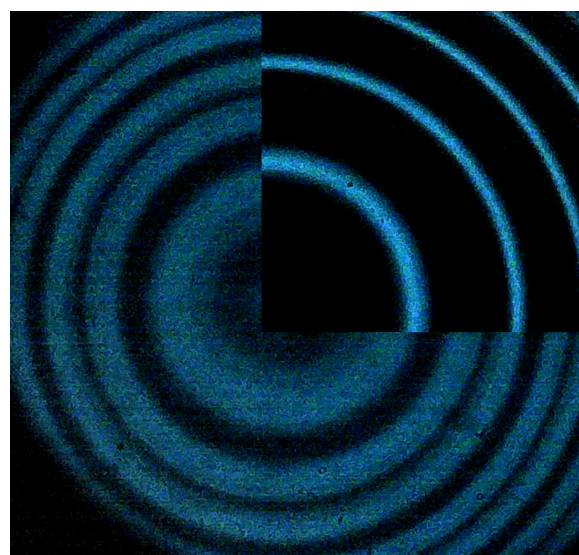


**Figure 15:** Approximation Method